

The flow and moisture fluxes associated with ridging South Atlantic Ocean anticyclones during the subtropical southern African summer

Thando Ndarana^{1,*}, Siyabonga Mpati¹, Mary-Jane Bopape²,
Francois Engelbrecht³, Hector Chikoore⁴

¹ Department of Geography, Geoinformatics and Meteorology, University of Pretoria, South Africa

² South African Weather Service, Centurion, South Africa

³ Global Change Institute, University of the Witwatersrand, Johannesburg, South Africa

⁴ Unit for Environmental Sciences and Management, North-West University, Vanderbijlpark, South Africa

*Correspondence: Thando Ndarana, Department of Geography, Geoinformatics and Meteorology, University of Pretoria, South Africa.
Email: thando.ndarana@up.ac.za

Abstract

Using 38 years of ERA-Interim reanalyses, this study examines the flow and associated moisture fluxes induced by ridging South Atlantic Ocean anticyclones over South Africa. The flow and moisture fluxes are divided into their geostrophic and ageostrophic components. Composite analysis reveals that ridging high pressure systems are modulated by Rossby wave trains that develop upstream in the middle latitudes near South America and the South Atlantic Ocean near the Greenwich Meridian. The wave trains are similar to those that are associated with tropical temperate troughs (TTTs) and nearly all TTTs are followed by ridging, whilst 20% of the ridging events are linked to TTTs. Composite analysis also shows that ridging-induced moisture fluxes affecting South Africa originate from different areas of the surrounding oceans at different times during the evolution of ridging highs. In the early stages, moisture enters the country along the southeastern coast through ageostrophic processes from a moisture divergence region located adjacent to the coast and remains largely south of 30°S latitude line. The moisture fluxes have a northeastern orientation on land, following the geometry of the eastern coast. These ageostrophic fluxes contribute to the occurrence of rainfall during the ridging process in the region located between Lesotho and Swaziland. Ridging events are associated with about 60% of rainfall days in summer over southern Africa whilst TTTs contribute about 21% summer rainfall days. During the later stages of the evolution of ridging, geostrophic fluxes enter the southern parts of Mozambique and contribute the accumulation of moisture in that region. The associated moisture divergence region is always located ahead of its ageostrophic counterpart, with a local maximum eventually forming in the Mozambique Channel.

Keywords: geostrophic and ageostrophic moisture fluxes, Ridging highs, precipitable water

1 INTRODUCTION

South Africa is primarily a summer rainfall region (Roffe et al., 2019) that is characterized by a pronounced zonal gradient in the precipitation climatology with more rain occurring in the

east (de Coning, 2013; Roffe et al., 2019). Rainfall in the far west and southwest coast of South Africa occurs during the winter months (Weldon and Reason 2014) and is influenced by cold fronts that are associated with mid-latitude cyclones being the main rain bearing weather systems (Mahlalela et al., 2019) whereas the south coast is an all season rainfall region (Weldon and Reason, 2014; Engelbrecht et al. 2015). Synoptic phenomena such as cut-off low (COL) pressure systems (Singleton and Reason, 2007; Favre et al. 2013;), upper air westerly troughs (Fravre et al. 2013) that propagate from west to east (Piva et al. 2010), tropical-temperate troughs (TTTs, Fauchereau et al. 2009; Ratna et al. 2013; Macron et al. 2014), tropical lows which contribute to rainfall in the Limpopo River basin (Malherbe et al., 2012; Rapolaki et al., 2019) and ridging South Atlantic Ocean anticyclones (Engelbrecht et al. 2015; Ndarana et al. 2018, referred hereafter simply as the ridging high) are the most important summer rainfall producing systems in the region. In addition to the synoptic scale rainfall processes, the eastern parts of South Africa and southern Mozambique experience mesoscale convective systems that contribute as much as up to 20% to the summer rainfall (Blamey and Reason 2012). For these weather systems to produce rainfall, moisture needs has to be transported into southern Africa mainly from the Indian Ocean or from tropical Africa.

Early studies of moisture transport (D'Abreton and Lindesay 1993; D'Abreton and Tyson 1995) showed that during early wet summers, moisture originates in the tropical oceans on both sides of the continent and converge over tropical southern Africa before it is transported southwards by eddies towards subtropical southern Africa. The eddies are defined as deviations from the basic state flow, which in D'Abreton and Tyson (1995), is considered to be the seasonal average. Only tropical Indian Ocean moisture flux divergence (MFD), with an associated moisture flux convergence (MFC) over the interior of South Africa is present during late wet summers. These MFD and MFC structures are associated with the north east African monsoon (Funk et al. 2016), which plays a critical role in east African rainfall.

The picture painted by D'Abreton and Tyson (1995) appears to be elucidated by the structure of moisture fluxes during the life cycle of TTTs (Ratna et al. 2013; Macron et al. 2014). After entering the western coast of the southern African subcontinent (in the Angola/northern Namibia region), moisture fluxes from the tropical Atlantic Ocean are organized towards the south east (Hart et al. 2010) by the Angola Low (Rouault et al. 2003; Reason and Jagadheesha 2005; Cr  tat et al. 2019; Howard and Washington 2018). In fact, the variability in the strength of the Angola low determines the moisture that becomes available for the cloud bands. Reason et al. (2006) suggest that when it is stronger, then there is more low level moisture in the source region for these cloud bands, and the opposite happens when it is weaker. These moisture fluxes play a significant role in wet spells over South Africa (Cook et al. 2004). This north-westerly moisture flux also amalgamates downstream with the north-easterly component from the tropical Indian Ocean and Mozambique Channel (Ratna et al. 2013; Macron et al. 2014), thus contributing to the moisture supply to the axis of TTTs. The latter moisture supply is stronger than the one upstream (Ratna et al. 2013). This moisture transport coincides with Inter-Convergence Zone (ITCZ) that migrates southward during the summer months (Suzuki 2011). Recent studies (e.g., Barimalala et al. 2018) have demonstrated that these moisture transport processes may also be substantially modified by changes in the cyclonic circulation processes in the Mozambique Channel. Even though a complete understanding of moisture fluxes is a work in progress, the advent of models with state of the art physical parametrization schemes (e.g., Ratna et al. 2014) means that the fluxes can be simulated more realistically (Vigaud et al. 2012).

Another source of moisture for South Africa is the Southwest Indian Ocean (SWIO, Dyson 2015). Ridging highs facilitate moisture transport into South Africa from the SWIO, based on forecasting experience, case studies and synoptic-type statistics (Triegaardt et al. 1988; Crimp and Mason 1999; Singleton and Reason 2007; Blamey and Reason 2009; Engelbrecht et al. 2015). In some instances, the southeasterly moisture flux occurs simultaneously with an upper-air trough or low causing vertical uplift and heavy falls of rain may occur as demonstrated by the studies referenced above. Cook et al. (2004) showed that wet spells are characterized or associated with increased moisture flux from the SWIO together with positive low-level geopotential anomalies over the eastern half of the country. The wet spells are also characterized by positive moisture divergence anomalies over the SWIO, with parts of the anomalies observed over land. Positive low-level geopotential anomalies over the eastern interior of South Africa and the SWIO have been clearly linked to the positive phase of the Southern Annular Model (SAM, Malherbe et al. 2014). Moreover, a positive trend in SAM has been observed in recent decades (Abram et al. 2014), and is projected to persist under low mitigation climate change futures (Zheng et al. 2013).

Figure 1 shows a 1979 to 2018 climatology of mean sea level pressure (MSLP) over the oceans surrounding subtropical southern Africa and 850 hPa geopotential heights over land that was derived from European Centre for Medium Range Reanalyses (Dee et al. 2011). A climatological anticyclonic circulation over the north eastern parts of South Africa (hereafter referred to as the north-eastern high pressure system) can be observed. The variability of this high pressure system is to some extent impacted by ridging high pressure systems (Ndarana et al. 2018), therefore the flow associated with it may play an important role in moisture transport or distribution processes during the evolution of the ridging process. This north-eastern high pressure system may also be affected by the easterly flow that is dynamically adjusted by the presence of southern Madagascar topographical structures, which also play a role in regulating the strength of the Mozambique Channel Trough (Barimalala et al. (2018). It also appears to be an extension of the Indian Ocean anticyclone (also known as the Mascarene high) and is least intense during the summer months when the Mozambique Channel trough is most clearly seen and most intense (Barimalala et al. 2020). However its role in moisture transport processes has not been considered in the literature. Therefore, the first objective of this study is to assess the role of the north eastern high pressure system in moisture transport processes by establishing the role that ridging highs play in this process. Secondly, the amount of rainfall that ridging high pressure systems bring into the country has not been quantified yet, except for the Cape south coast in Engelbrecht et al. (2015). This is largely due to the fact that studies that use objective methods to identify these systems are lacking in the literature. Finally the relationship between ridging highs and TTTs has been mentioned in studies that consider the latter (Fauchereau et al. 2009; Hart et al. 2010; Ratna et al. 2013; Macron et al. 2014) but the extent of this relationship is still an open question. This study will render this relationship more explicit.

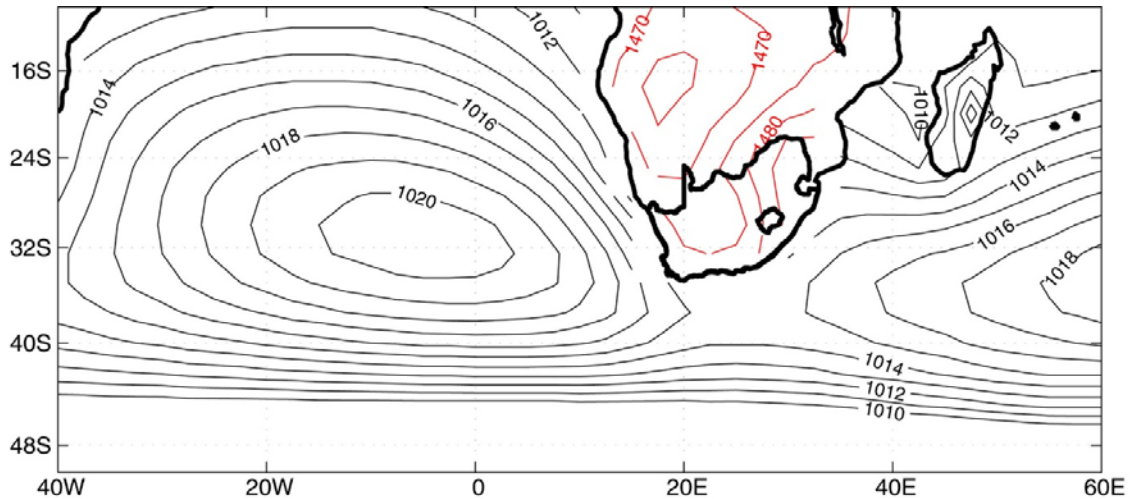


FIGURE 1. December to February climatology of mean sea level pressure (black contours over the ocean) and 850 hPa geopotential heights (red contours over southern African mainland) plotted with 1 hPa and 10 gpm contour intervals, respectively. The figure was produced using ERA-interim reanalysis data sets for the 1979 to 2018 period

The paper is structured as follows: In the next section the data and methods are discussed, followed by the results in Section 3, which includes Rossby waves and ridging highs, the composite evolutions of ridging highs and associated moisture flux processes, given the flow conditions that are induced by the ridging process and the contribution that ridging highs make to southern African rainfall. The concluding remarks are presented in Section 4.

2 DATA AND METHODS

2.1 Data

To identify ridging South Atlantic Ocean high pressure systems during the summer (December – February [DJF]), we use the European Centre for Medium-Range Weather Forecasts (ECMWF) (Dee et al. 2011) and the Japanese 55-year (Kobayashi et al. 2015) reanalyses products from 1979 to 2018, hereafter referred to as ERA-Interim and JRA-55, respectively. Dessler and Davis (2010) showed that there is good agreement between the two datasets considered for this study, whereas other reanalysis products exhibited more extensive biases. The choice using ERA-Interim and corroborating the results with JRA-55 reanalysis is also informed by the fact that these two products were produced using the 4 dimensional variational data assimilation, which as far as we know, is the most advanced data assimilation method at present. This is quite an important issue to contend with for a region that is as data sparse as Africa. We apply both data sets at a horizontal grid spacing of 2.5° in latitude and longitude, and at 6-hourly time intervals. Even though these products are available at finer mesh grids, we deem the chosen grid spacing sufficient because ridging high pressure systems are synoptic scale processes, the horizontal scale of which is $\sim 10^6$ m (Holton and Hakim 2014). The variables used are mean sea level pressure (MSLP), geopotential heights to calculate the geostrophic and ageostrophic wind fields and the specific humidity (q).

We also use CPC Global Unified Precipitation data provided by NOAA/OAR/ESLR PSD, Boulder, Colorado, USA.¹ This data is provided on a 0.5° horizontal grid spacing, daily from

1979 to 2018. Daily data is well suited for this study because individual weather systems and associated rainfall fields will be considered.

2.2 Methods and diagnostics

The method for identifying ridging highs is discussed in detail in Ndarana et al. (2018); only a brief description is provided here. It is a 3-step algorithm that identifies closed MSLP contours and then groups all those that are concentric together such that the contour levels of MSLP increase inward. The concentric contours would then belong to the same anticyclone. Ridging highs are defined as all those anticyclones that extend eastward and cross the 25°E latitude line. If this condition is met for consecutive days, with no days violating it in between, then all the anticyclones that meet the condition belong to same ridging high event. On the basis of this, the duration of the events can then be calculated. Concentric contours with the largest contour entirely east of the 25°E latitude line are considered to be part of or are the Indian Ocean high pressure system. Ridging events begin in the South Atlantic Ocean and the process completes in the Indian Ocean; for this reason the domain of interest is bounded by 40°W and 60°E and by 10°S and 50°S. To establish the climatological behaviour of ridging events, we use composite analysis. For instance, the MSLP and other fields for events that have a 3- day duration are organized such that the days of inception of the ridging process coincide, which is then followed by the averaging. In all plots showing the lagged composites of ridging highs, day 0 corresponds to the first day that the South Atlantic high pressure system extends eastward.

We also employ a slightly modified and more relaxed version of the TTT index (Ratna et al. 2013) to objectively identify TTT events during the study period. The aim of opting to relax the conditions of the index is to attempt to identify all instances of outgoing longwave radiation (OLR) that have the dipole structure similar to those in Fauchereau et al. (2009), Ratna et al. (2013) and Macron et al. (2014). In this study we require only that $(OLR_{E1} + OLR_{E2})/2$ and V_W be positive, $(OLR_{W1} + OLR_{W2})/2$ and V_E be negative. The reader is referred to Figure 2(a) in Ratna et al. (2013) for the meanings of these variables. In all lagged composites involving TTTs as defined here, day 0 corresponds to the day before the first day that these conditions are satisfied, which Ratna et al. (2013) defined as the onset of the mature stage of TTTs.

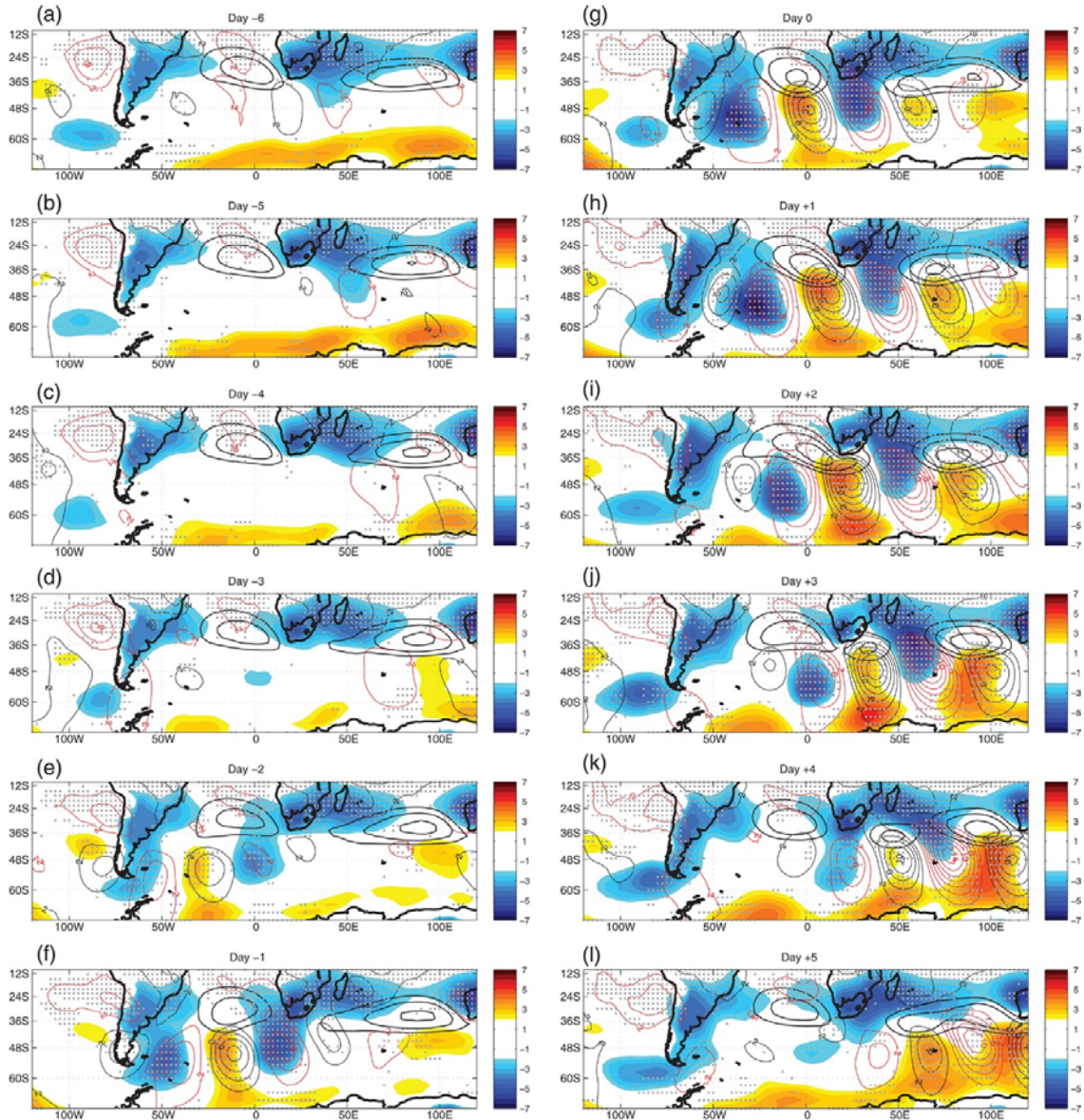


FIGURE 2. Lagged composites of MSLP (thick black contours), negative (positive) perturbation meridional velocity represented by the this red (black) contours and negative (positive) anomalies of MSLP represented by the blue to dark blue (yellow to dark brown) shading. The outer, middle and inner thick black represent the 1,017, 1,018 and 1,021 hPa, respectively. The grey dots represent grid points where both the perturbation meridional velocity and MSLP anomaly fields are significant at the 95% confidence level. the composites are plotted from (a) day -6 to (l) day +5. The composites were produced using DJF ridging high pressure systems from 1979 to 2018

The approach to diagnosing moisture fluxes adapted in this study is slightly different from those considered in previous ones, some of which decompose the moisture flux fields into stationary and transient components (e.g., Vigaud et al. 2007). In this approach, the diagnostics would have to be averaged in time (or zonally) over the entire event, resulting in constant values right through its evolution, or zonally aggregated diagnostics in the case of zonal averaging. Other studies (e.g., D’Abreton and Tyson 1995; Behera et al. 1999; Todd et al. 2004, Ratna et al. 2013) decompose the vapour flux vector into the nondivergent and irrotational components. This approach requires that the Poisson equations that materialize in

this framework be solved to obtain a streamfunction and a potential function of the fluxes, which is not straight forward to interpret and directly link to the flow. Difficulties associated with the above mentioned methods suggest that a different approach be adopted. Since the objective of the current study is to assess the impact of a specific individual synoptic weather system on moisture transport, and also given the fact we employ composite analysis, we proceed to separate the moisture transport processes into fluxes by the geostrophic and ageostrophic wind fields and integrate them vertically as follows:

$$\begin{aligned}
\mathbf{Q} &= \frac{1}{g} \int_{600}^{p_s} q \mathbf{V}_h dp \\
&= \frac{1}{g} \int_{600}^{p_s} q \mathbf{V}_a dp + \frac{1}{g} \int_{600}^{p_s} q \mathbf{V}_g dp \\
&= \mathbf{Q}_a + \mathbf{Q}_g
\end{aligned} \tag{1}$$

where \mathbf{V}_h , \mathbf{V}_g , \mathbf{V}_a , q , p_s and g are the horizontal flow, geostrophic wind, ageostrophic wind, specific humidity, surface pressure and gravitational acceleration, respectively. Note that the integration is calculated up to 600 hPa, as in Xue et al. (2018), because the flow over the Indian Ocean that is associated with ridging highs changes completely beyond this level to become sinusoidal and westerly, even as the flow in the lower levels is south-easterly. Other studies integrate the fluxes to 300 hPa (e.g., Chen 1985).

The advantage of this approach is that the moisture flux dynamical processes that are associated with the north-eastern high pressure system (Figure 1) can more easily be discerned. They are also better linked to effects of the flow on moisture fluxes and their divergence. The ageostrophic wind is defined as $\mathbf{V}_a = \mathbf{V}_h - \mathbf{V}_g$. This means that the ageostrophic wind depends on how the geostrophic component of the flow is defined, which is one of two ways. The first is geostrophy-0, where the Coriolis parameter is kept constant at a reference latitude and geostrophy-1, in which case the Coriolis parameter varies with latitude (Blackburn 1985). In this study the latter is adopted, and as such, the geostrophic wind is not nondivergent ($\nabla \cdot \mathbf{V}_g = -(\beta/f)v_g$, Cook 1999)). Therefore both the geostrophic and ageostrophic flows induce vertical motion, as dictated by the conservation of mass (Holton and Hakim 2014), and may contribute to the production of rainfall, if sufficient moisture available is (Doswell III et al. 1996).

Lim et al. (1991), Kwon and Lim (1999) and Holton and Hakim (2013) decomposed the ageostrophic flow into the isallobaric wind and the component representing advective effects (i.e., $\mathbf{V}_a = f^{-1} \mathbf{k} \times (\partial \mathbf{V}_g / \partial t) + f^{-1} \mathbf{k} \times (\mathbf{V}_g \cdot \nabla) \mathbf{V}_g$). In addition, due to the local increase in the strength of the geostrophic flow (first term on the right of this expression), the geopotential tendencies have implications for the development, structure and orientation of the ageostrophic flow. This will be used to motivate the ageostrophic vector field that is induced by the ridging process.

3 RESULTS

3.1 Modulation of ridging highs by Rossby wave trains and associations to TTTs

The main method of analysis in this study is lagged composite analysis in which events of the same duration are grouped together. A total of 699 DJF ridging events were identified in ERA-Interim re-analysis during the 38-year study period. The number of events is

corroborated by the 697 events that were also identified in JRA-55 data. The number of events decreases nearly exponentially (Ndarana et al. 2018) as a function of their duration and the centres of the events are confined between 25°S and 45°S. This influences the simplicity of the compositing method. Ridging anticyclones are most clearly seen by examining MSLP contours. For clarity, we only show a few MSLP contours in Figure 2, together with the MSLP anomalies (shaded) and the perturbation meridional component of the 200 hPa wind field (thin black and red contours). The latter two fields combined diagnose Rossby wave trains and the baroclinic structure of these waves.

Ridging high pressure systems appear to have a spatial and temporal relationship with Rossby wave trains. From about three days before the eastward extension of the South Atlantic anticyclone, a baroclinic disturbance develops west of the southern tip of South America, just west of Drake Passage. A secondary component of the wave train develops near the Greenwich Meridian. The Rossby wave intensifies as it propagates north-eastward towards the South African domain and the initiation of the ridging process coincides with positive MSLP anomalies as the latter propagates past the country and associated southward meridional excursions of air parcels aloft (red contours to the west of South Africa). The development and propagation of the Rossby wave trains are very similar to those described in O'Brien and Reeder (2017), even though the waves in that study exhibit a higher degree of wave reflectivity. Its eastward propagation is along the midlatitude waveguide (Ambrizzi et al. 1995) that is provided by the midlatitude jet (O'Kane et al. 2016). The co-occurrence of ridging high pressure systems and synoptic scale Rossby waves shows that the ridging process occurs in a baroclinically unstable atmosphere, because the waves are tilted westward with height.

Ratna et al. (2013) showed that TTTs are also associated with Rossby wave propagation. The difference between the Rossby wave trains in Figure 2 in the current study and those of Ratna et al. (2013) is that the latter appear to be quasi-stationary. Moreover, the meridional excursions of air parcels that characterize air parcel oscillations during Rossby wave propagation (Holton and Hakim 2014) are in opposite directions over South Africa during the occurrence of TTT and ridging highs. The inception of ridging is associated with poleward excursion of air parcels downstream of South Africa (Figure 2 [h]) and when the bean shaped structure is formed, on day +2 (Figure 2 [i]) then the air parcels excursions become equatorward. The bean shape in the MSLP contours is indicative of a maturing ridging high process, which is immediately followed by a break off of the leading edge of the South Atlantic high that later amalgamates with the Indian Ocean high pressure system. In contrast, the eddy meridional wind values over South Africa during the TTTs are negative.

The Rossby wave signature suggests that TTTs might be followed by ridging. Figure 3, which was produced using TTTs that were identified using a more relaxed TTT index, demonstrates this. The familiar OLR structure (Fauchereau et al. 2009; Ratna et al. 2013; Macron et al. 2014) that is characteristic of TTTs begins to form on day -3 and on day -1, the anomalous moisture fluxes are north westerly and similar to those shown in Figure 10 in Macron et al. (2014) and the low level flow presented in Figure 9 in Ratna et al. (2013). We consider days -3 to -1 the development stages of the TTT events (Ratna et al. 2013). Figure 3 also reveals the behaviour of the South Atlantic high pressure system as TTTs mature. It begins its eastward extension on day -1 and on day 0 the bean shape forms, displacing the north-easterly flow eastward, deeper into the Indian Ocean, to allow onshore flow in the region where the negative OLR anomalies are located. Ratna et al. (2013) considered day 0 as the onset of the matured stage of the TTTs and they dissipate as the leading edge of the South

Atlantic high breaks off to amalgamate with the Indian Ocean high and the anomalous onshore moisture fluxes, which are statistically significant at the 95% confidence level (Brown and Hall 1999), strengthen considerably. The relationship between ridging highs and TTTs has been mentioned in previous studies (but had not been made explicit before).

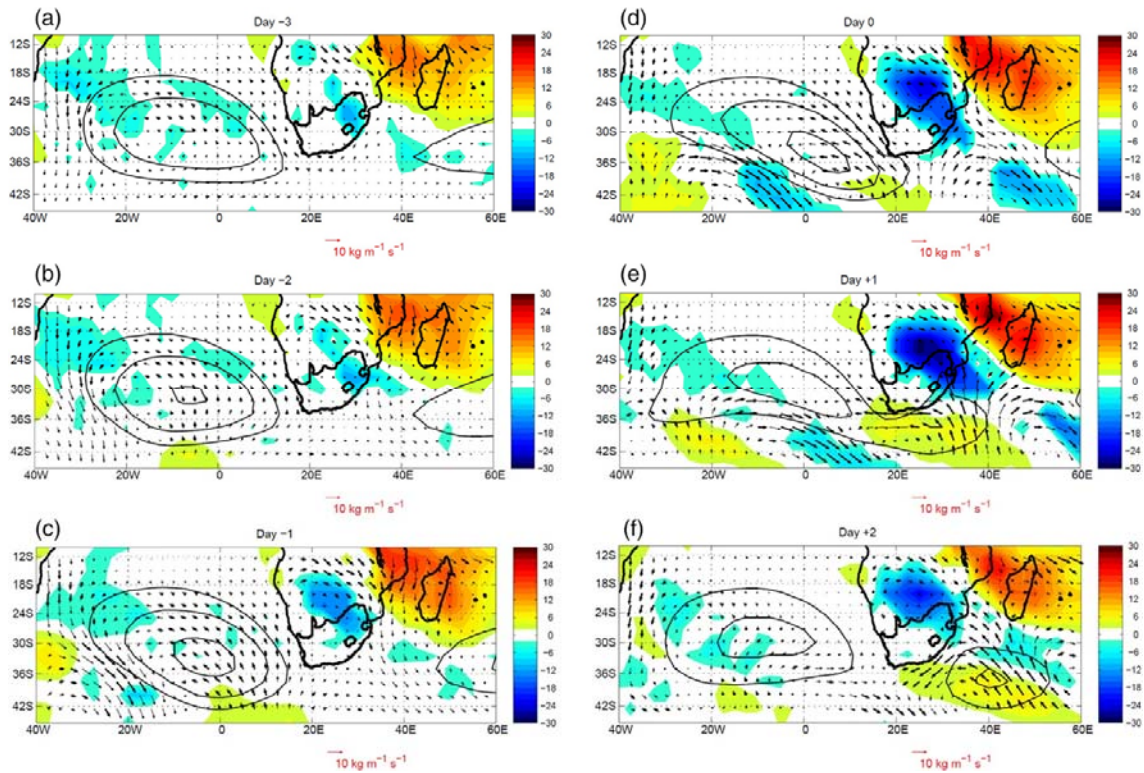


FIGURE 3. Lagged composites of negative (positive) anomalies of OLR represented by the blue to dark blue (yellow to red) shading and anomalies of low level moisture fluxes integrated between the surface and 600 hPa represented by the black contours. The thick black contours represent the 1,017 (outer), 1018 (middle) and 1021 (inner) hPa. Day 0 (the onset of the maturing stage) correct the day before the first day on which all the TTT index conditions are satisfied. only OLR anomaly fields that are significant at the 95% confidence level are shown and the thick black arrows represent the moisture fluxes that are significant at the 95% confidence level. the composites were produced using DJF ridging high pressure systems from 1979 to 2018

Whilst Figure 3 demonstrates that many of the TTT events have a ridging event associated with them, the question of whether all TTTs events do remains unanswered. The automatic appearance of the ridging process when TTTs are composited together shows that the majority of the latter are associated with the former. Since the development stage of TTT precede the ridging process as shown by the evidence discussed above, for each day from day 0 of the TTT, we search for an associated ridging event. We find that almost all the TTTs identified in this study are associated with ridging highs, thus confirming the result of the composites, whilst only about 20% of the latter are linked to TTTs. Previous studies of TTTs have indirectly addressed the role of ridging highs but this relationship had not been made explicitly and quantified.

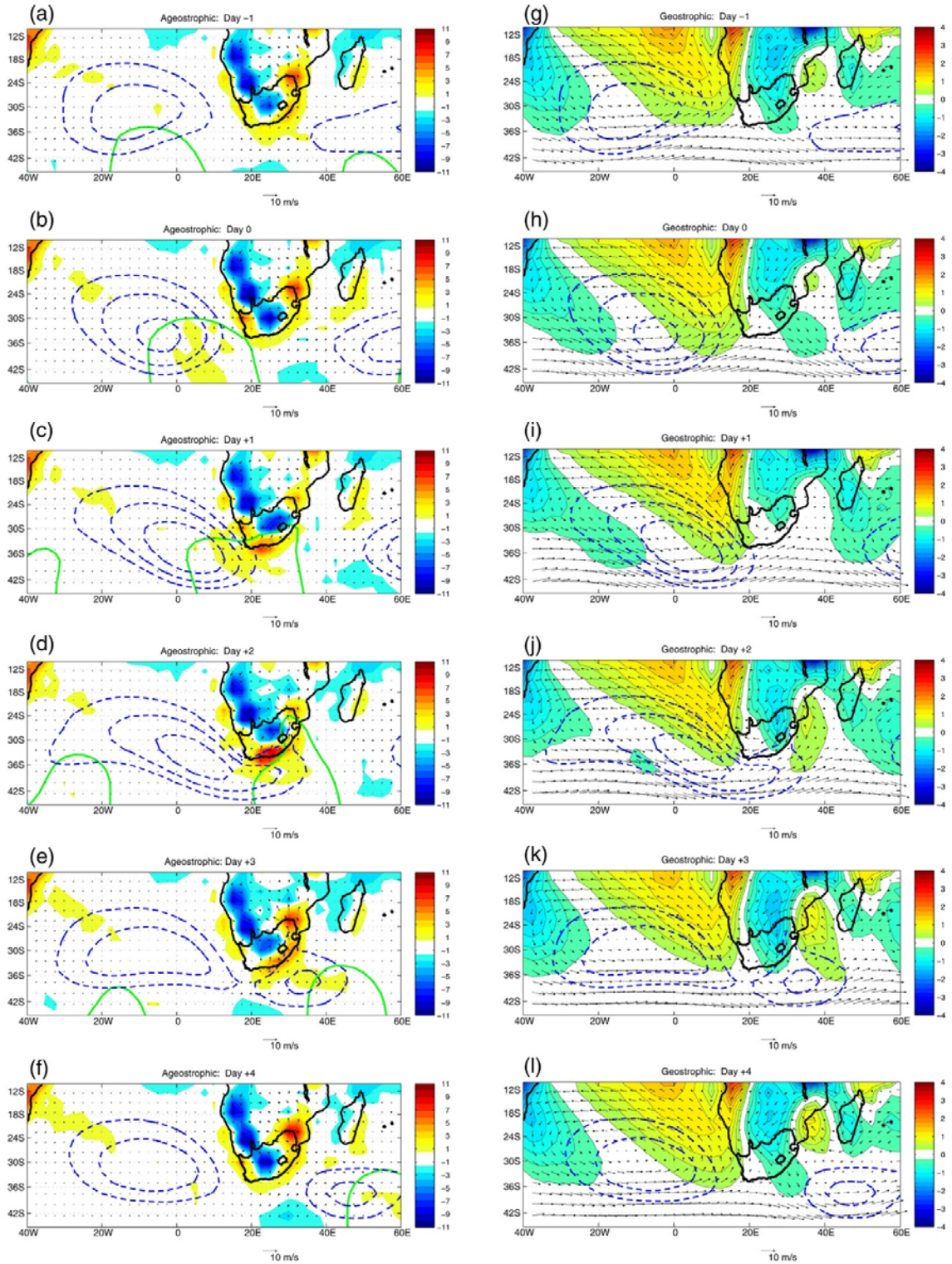


FIGURE 4. Lagged composite evolution of the 850 hPa geostrophic (left panels) and ageostrophic (right panels) wind together with their divergence (brown shading) and convergence (blue shading) fields. The vector scale is 10 m s^{-1} and the shading plotted at 10^6 s^{-1} . The thick blue dashed contours represent the 1,017 (outer), 1018 (middle) and 1021 (inner) hPa MSLP contours. The thick green curve is the 10 m day^{-1} . The evolution of the fields begins from (a, g) one day before the inception of the ridging process (day -1) to (e, j) the day after the ridging ceases (day $+4$). The composites were produced using DJF ridging high pressure systems from 1979 to 2018

3.2 Ridging highs and the associated flow

Composite evolution of the MSLP fields together with 850 hPa geopotential tendency fields show that as ridging evolves and the leading edge enters the eastern parts of South Africa, a region of positive geopotential tendencies develops along the eastern interior of the country. For clarity and relevance to the discussion below, we only show one green contour of the positive geopotential tendency field in the left panels of Figure 4.

The geopotential tendency fields play an important role in determining the structure of the ageostrophic flow vector field that occurs during the evolution of ridging events. The ageostrophic flow and its divergence (left panels of Figure 4) are different in pattern from their geostrophic counterparts (right panels of Figure 4). First, the ageostrophic flow divergence is more localized with a maximum that is confined along the coast, right through the evolution of the ridging highs. It develops and strengthens near the southwestern tip (Cape Town area) at day 0 (Figure 4(b)), and then propagates in a northeastward direction, following the coastline as it strengthens. It then enters the country to eventually coincide with the high-pressure system over the north-eastern parts of South Africa (Figure 1), at the end of the ridging process. Pronounced ageostrophic flow convergence is also found and is dominant over the western half of the country. This broad pattern of convergence and divergence is consistent with flow occurring from the coastal regions where the highs are ridging towards the trough present over the western interior.

The direction of the ageostrophic flow is mostly northeastward and is consistent with the positive geopotential tendency field (the green curve, which represent the $10 \text{ m}^{-2} \text{ s}^{-1} \text{ day}^{-1}$ contour). It is also consistent with the flow divergence and convergence patterns. We expect from the idealized model of the low level ageostrophic wind in baroclinic waves (Lim et al. 1991; Kwon and Lim 1999; Holton and Hakim 2013), that the flow will point away from the centre of positive geopotential tendencies. This is the case in Figures 4 (b) to (d).

As noted in Section 2, the ageostrophic flow may be decomposed into isallobaric and advective components. The largest Eulerian acceleration of the geostrophic flow occurs on land, precisely where the ageostrophic flow increases from one time step to the next (Figure 4). Composites of the isollabaric wind (not shown) suggest that, in particular Eulerian acceleration of the zonal component of the geostrophic wind ($\partial u_g / \partial t > 0$), which spatially coincide with the arrows representing the ageostrophic wind, contributes the most to these increases. This shows that the magnitude of the latter is informed by the former.

Finally, the form of the geostrophic flow used in this study is not non-divergent. Examination of Figures 4(g) to (l) shows that before the inception of ridging at day 0, there is weak geostrophic convergence in the SWIO. As the ridging evolves and matures, flow divergence extends from the South Atlantic Ocean, eastward following the MSLP isobars, as they extend eastward also. From day +2, the geostrophic flow divergence dominates in the SWIO, with a local maximum found in the Mozambique Channel. Overland, flow convergence extends south, forming a tongue that dominates much of South Africa. The geostrophic flow, represented by the arrows, is consistent with the flow divergence/convergence fields. It starts off parallel to the coast (see Figure 4 (h) to (i)), and then turns anticyclonically, to enter the country north of 30°S (Figures 4 (j) and (l)). The flow entering the country originates from the SWIO flow divergence just described, and it continues to turn anticyclonically into the interior of the country.

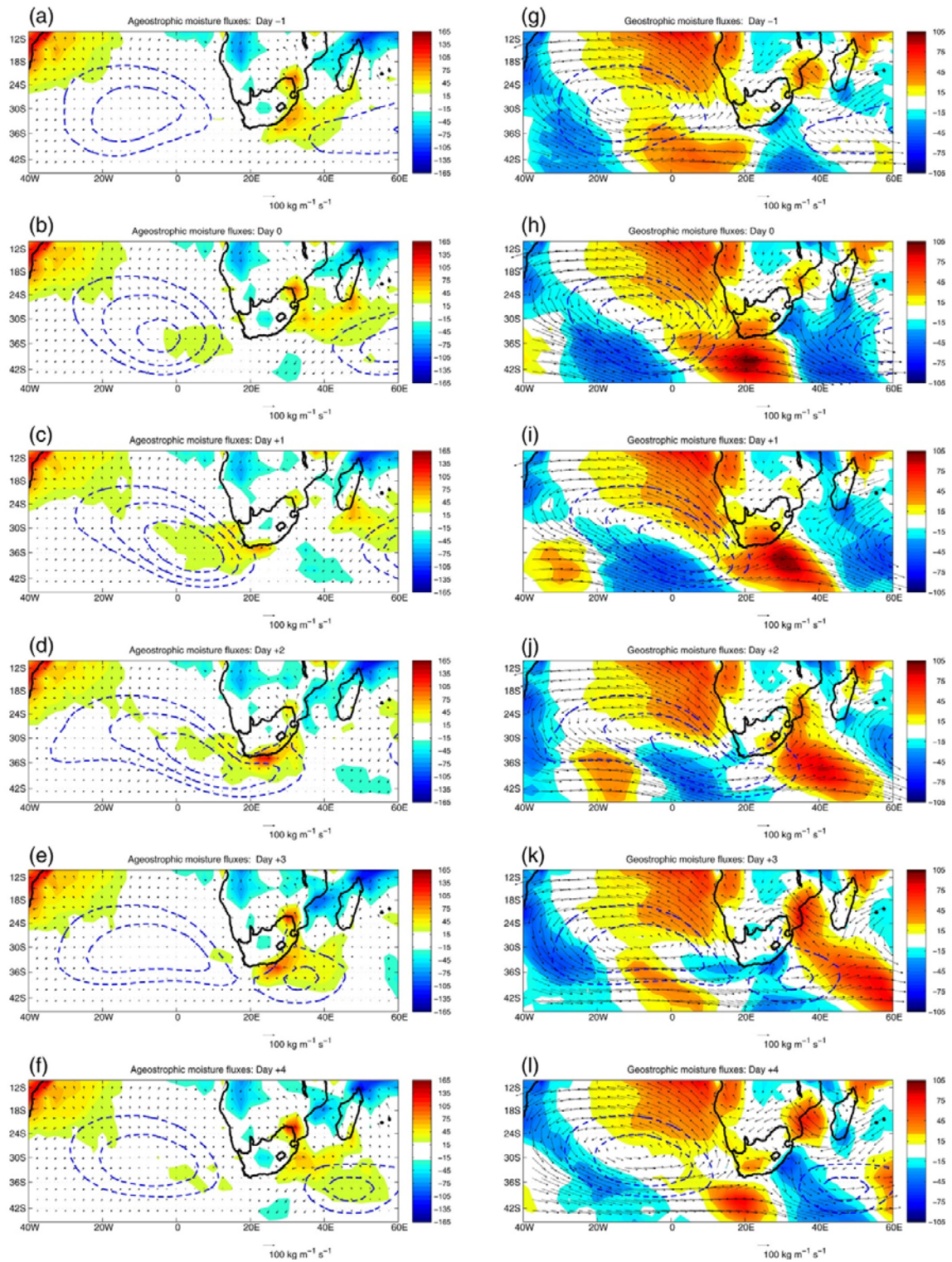


FIGURE 5. Same as in Figure 4 but for low level, vertically integrated ageostrophic (left panels) and geostrophic (right panels) moisture fluxes

3.3 Influence of ridging on moisture fluxes

Comparing the corresponding panels of Figures 4 and 5 shows that the ageostrophic and geostrophic moisture fluxes and their divergence/convergence patterns are influenced by the respective flows, which are in turn induced by the ridging process. At the earlier stages of ridging (day 0 to +2) moisture enters the country by means of ageostrophic processes along the south coast and some via geostrophic fluxes but at later stages (day +3) onshore moisture fluxes become purely ageostrophic along the south eastern coast. These onshore ageostrophic moisture fluxes always occur south of the 30°S latitude line and the divergence region associated with them also remains south of this line. This moisture divergence region is located adjacent to the land mass, as opposed to further off shore, as it is the case with its geostrophic counterpart. The moisture that enters the country via these fluxes is then transported in a northeastward direction, following the geometry of the eastern coast. Because of the similarity of the ageostrophic fluxes and their divergence patterns to the respective flow, we may conclude that these fluxes are influenced by the ridging process; since the flow has been shown to be induced by it in the previous section.

As the ridging process enters the north eastern parts of the country, the ageostrophic flow from the south transports moisture into the high pressure system that is located over the north eastern part of South Africa, whilst there are fluxes of moisture out of it, on the north end. The latter appear to be taking moisture out of the high and distributing it in all directions from the northwest to the north east. Note that the pattern in Figure S1 takes form towards the maturity of the ridging process. The secondary ageostrophic moisture divergence region found on land is caused by the development of the north-eastern high pressure system.

The geostrophic moisture flux divergence (right panels Figure 5) is similar to the total moisture flux (not shown) and the fluxes are parallel to the south eastern coast at the earlier stages of the evolution of ridging highs but enter the country in a similar way as the total fluxes at the later stages. The geostrophic moisture divergence remains ahead of its ageostrophic counterpart and the former elongates and breaks into two centres. A smaller localized maximum moisture divergence eventually reaches the Mozambique Channel and a larger one remains in the SWIO. As the ridging enters South Africa over the eastern coast, the geostrophic fluxes associated with the Mozambique Channel divergence enter the country over the southern parts of Mozambique. This also is influenced by the geostrophic flow. After their entrance on land, the fluxes turn anticyclonically around the high pressure system located over the eastern interior of the country. We have not considered the interaction between the ridging high and the Mozambique Channel Trough. This is an issue planned for later in a modelling study. A study by Chikoore et al. (2015) has also shown that the complex Madagascar topography induces vortex enhancement in the trough due to topographic shearing, which may also affect moisture fluxes.

This discussion shows that the high pressure system located in the eastern interior plays two roles that cannot be seen when composites of the total fluxes (not shown) are examined. These roles are most clearly seen when the flow and the associated fluxes are separated into their ageostrophic and geostrophic components. Furthermore, by decomposing the flow, we have characterized the dynamical nature of the moisture fluxes and where in the Indian Ocean this moisture originates during the evolution of ridging highs. The eastern coast and eastern interior of South Africa receives its moisture from waters that are adjacent to the land via the ageostrophic flow, whereas the moisture the sub-continent receives further north occurs as a result of fluxes that enter Mozambique largely through geostrophic processes. Some of this

geostrophic moisture appears to penetrate towards Botswana and Namibia where it may contribute to TTTs. All this might have important applications in short to medium forecasting and diagnosing heavy rainfall events that affect South Africa's eastern KwaZulu-Natal province, thus improving the predictability of rainfall in the region. For forecasting at these time scales, post processing procedures that will explicitly produce forecasts of ageostrophic moisture fluxes and divergence could be developed and operational forecasters could incorporate this information into their decision making processes about rainfall over the eastern parts of South Africa. The results presented in Figures 4 and 5 were produced using ERA-Interim reanalysis data. Similar results were produced (not shown) using JRA-55 data to corroborate these.

3.4 Rainfall anomalies associated with ridging highs

In this section we consider the impact of ridging high pressure systems on rainfall over South Africa and consider the benefit of decomposing the associated moisture fluxes into their ageostrophic and geostrophic components discussed in the previous subsection. Figure 6 shows lagged composites of rainfall anomalies (shading), which are calculated by subtracting the 1979/1980 to 2017/2018 DJF climatology (expressed in mm/day) from the daily rainfall fields. Superimposed on the rainfall anomalies, precipitable water anomalies significant at the 95% level are also included, as represented by the dark grey dots. These anomalies are also consistent with and are predicted by their rate of change, which measures moistening during the ridging process. Therefore the moistening is not constant as ridging evolves.

Prior to the inception of the ridging process, the rainfall anomaly composites show that the South African domain is relatively dry. Once ridging has commenced, positive anomalies develop over the eastern parts of the land, and progressively spread northward as well as migrate towards Mozambique, largely following the coast. The precipitable water anomalies are in broad agreement with the rainfall anomalies. They attain their highest values in Mozambique. Inspection of the total moisture fluxes (not shown) and comparing them to the geostrophic moisture fluxes in Figure 5 demonstrates that the rainfall occurrence in Mozambique is explained by the latter and therefore largely influenced by the geostrophic flow in that region. The results shown in Figure 6 are for ridging events that have a 48 hour duration, but similar results for longer lived events were observed. The behaviour of the rainfall and the associated statistically significant precipitable water that are associated with shorter lived events are also consistent with the behaviour of the ridging events. The difference between the shorter and longer lived events is that the latter's anomalies migrate all the way into the western boundaries of the Mozambique Channel and the former do not do so as much.

However, right through the evolution of the ridging process, the total moisture fluxes are offshore over the eastern coast of South Africa, particularly in the KwaZulu-Natal Province of the country. The orientation is the opposite of what one expects for rainfall to be produced in that part of the country. It is only when we decompose the moisture fluxes into their ageostrophic and geostrophic components that the impact of moisture transport from the SWIO becomes clearer. The rainfall anomalies on day 0 (Figure 6 (d)) are influenced by northeastward ageostrophic fluxes seen in Figure 5 (b). As the extension of Atlantic high pressure system begins, its bean shape forms on day +2, the rainfall anomalies increase in magnitude in the north eastern parts of South Africa. This increase appears to be largely influenced by ageostrophic processes which bring moisture from parts of the SWIO that are adjacent to the country.

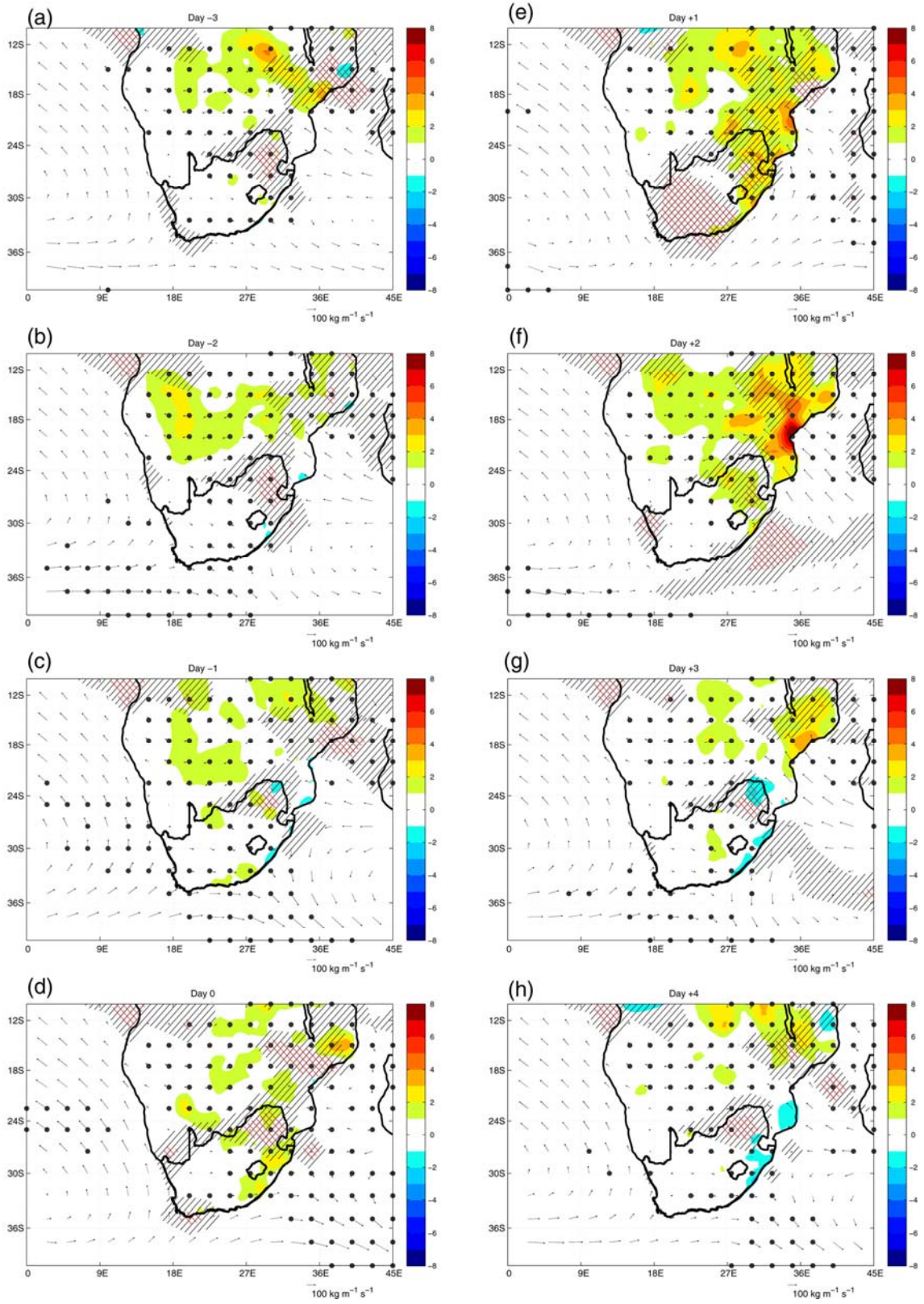


FIGURE 6. Composites of rainfall anomalies (shaded) during the evolution of ridging high pressure systems, beginning from 3 days before the onset of the ridging process on (a) day -3 to the day after it has ceased. the black (red) hatched with lines oriented at 45° (135°) to the horizontal represent regions where $|Q_a|/|Q_g| > 0.5$

(>1). The arrows represent moisture fluxes by the total flow. The dark grey dots represent grid points at which positive anomalies of precipitable water are statistically significant at the 95% significance level

The relative strength of the ageostrophic fluxes relative to their geostrophic counterparts is quantified by the non-dimensional ratio. The region hatched with black lines represents the area where this non-dimensional ratio greater or equal to 0.5 and that which is hatched area with red lines represents areas of the ratio values greater or equal to 1. This shows that the ageostrophic fluxes play a significant role in bringing moisture into the country and over the eastern central parts of South Africa and these fluxes are more dominant than the geostrophic ones. It follows then that to more accurately diagnose moisture transport processes that influence the KwaZulu-Natal region it is necessary to decompose these velocity field in the manner proposed here.

In Section 3.1 we showed that almost all TTTs are followed by ridging high pressure systems. This sequence of events plays a critical role in the distribution of rainfall, as shown in Figure 7, which should be read together with Figures 3 and 6. Before considering the issues of air mass instability and uplift associated with widespread rainfall, the rainfall anomaly patterns associated with the TTT and the ridging high days are described. The obvious difference between the rainfall anomalies associated with ridging highs and those that are associated with TTTs is that the latter are more widespread. Figure 7(a) shows positive anomalies at and near the east coast, which intensify by day +1 (Figure 7(e)), as the OLR anomalies become stronger and ridging occurs (Figure 3(e)). Positive rainfall anomalies also appear in southern and central Mozambique and are influenced by the ridging induced geostrophic moisture fluxes, as described in Subsection 3.3. This is clearly an impact of ridging highs that occurs at this point of the evolution of TTTs (Figure 3 (e)). As ridging matures and dissipates, which is signalled by the leading edge of the South Atlantic high having been broken off from the parent anticyclone (Figure 3 [f]), TTT rainfall migrates northward. This migration is brought about by the northward movement of onshore moisture fluxes that are influenced by the ridging process. The evolution of the rainfall anomalies is consistent with that of OLR anomalies in Figure 3, and corresponds to Regimes #5, #6 and #7 in the cluster analysis of Fauchereau et al. (2009) and Macron et al. (2014). The negative OLR indicates enhanced convection, and therefore some of the rainfall anomalies will be convective and correspond to mesoscale convective complexes in the region (Blamey and Reason 2012).

Dyson and van Heerden (2002) partly used moist static energy (MSE) to develop a model for identifying tropical weather systems over South Africa and found values of MSE beyond a particular threshold value (positive MSE anomalies) coincided with heavy rainfall over the country. A similar relationship has also been found in the composite of MSE anomalies (not shown) that correspond to Figures 6 and 7 in this study. The MSE anomalies appear to be influenced by moisture transport, meaning the L_q plays the most significant role in contributing to atmospheric instability, as defined by MSE.

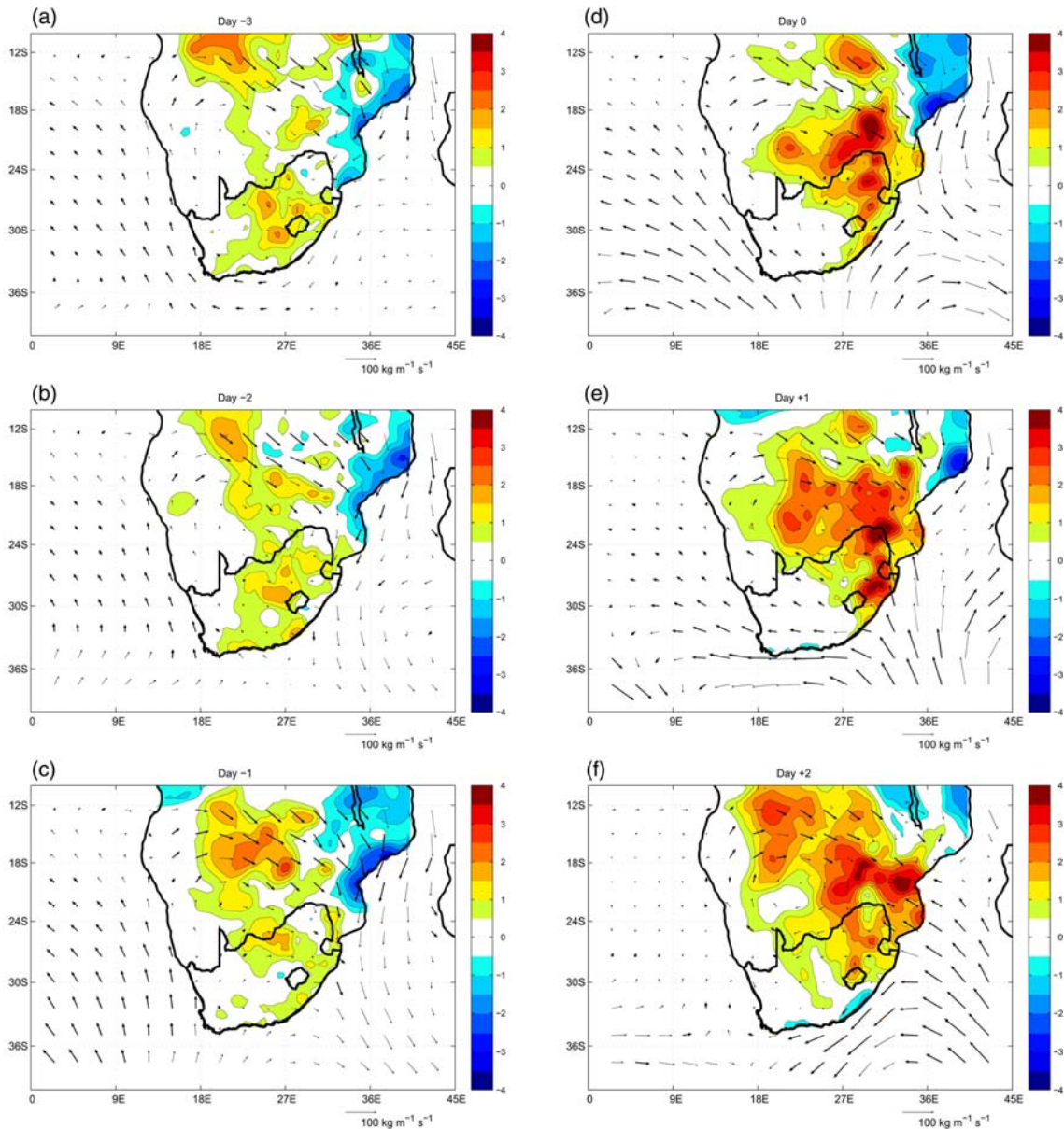


FIGURE 7. Same as in Figure 3 but the OLR anomalies are replaced by the rainfall anomalies, the domain is zoomed into and the MSLP contours have been omitted

The remaining issue is the amount of rainfall that ridging high pressure systems contribute to the southern African domain, with the understanding that these systems are not rainfall producing systems per se, but as demonstrated above, they facilitate the influx of moisture from the SWIO and a lifting mechanism would have to be present over the country, that is provided by cut-off lows (e.g., Favre et al 2013), for instance or uplift as a result of orography. The systematic identification of these systems enables this. For each season we calculate the cumulative rainfall from the beginning of December to the end of February over the southern African domain (rainfall occurring over land up to 15°S – based on the composites of negative OLR anomalies (Figure 3) and rainfall anomalies (Figures 6 and 7), and compare it to the cumulative rainfall on days when there are ridging highs, but excluding the days on which the ridging highs are associated with TTTs because we consider the ridging highs that are associated with the TTTs to be part of those systems.

We estimate the number of rainfall days that are associated with ridging highs and TTTs. The former exclude all those events which have been found to have associations with the latter. First we calculate the daily area averages rainfall south of 15°S. The choice of this cut off latitude is informed by the OLR anomalies in Figure 3 (seen also in previous studies (Fauchereau et al. (2009), Ratna et al. (2013) and Macron et al. (2014)) and the rainfall anomalies in Figures 6 and 7. The number of days during which rainfall anomalies are recorded for each season and for each year is then calculated when there are ridging highs and when there are TTTs. In the ridging high case the rainfall days, as defined above, is calculated from day 0 to the end of the ridging process and in that of the TTT it is calculated from day -3 to the last day that the TTT index condition (Section 2) is complied with. We find that ridging high pressure systems contribute 60% to summer rainfall days per year, where TTTs contribute about 21% of these. This stands to reason because there are many more ridging high events than there are TTTs (Subsection 3.2). Moreover, the former have to be associated with many types of upper level synoptic weather systems that provide the lifting mechanism to produce rainfall over South Africa. The TTT is one such synoptic weather system.

4 CONCLUSIONS

In this study, 38 years of ERA-Interim reanalysis dataset was used to investigate the relationship between the flow and moisture fluxes that occur during the evolution of ridging South Atlantic Ocean anticyclones over southern Africa. The relationship between Rossby wave trains, TTTs and ridging highs was also investigated. The results were corroborated using JRA-55 reanalysis. The study focused on the austral summer months, namely December to February. To diagnose moisture fluxes, the low level flow was divided into its ageostrophic and geostrophic-1 components.

It was shown in this study that ridging high pressure systems are modulated by Rossby wave trains that develop in the middle latitudes over the eastern parts of the South Pacific Ocean near the southern-most tip of South America and in the South Atlantic Ocean. Whilst the ridging high pressure systems themselves are not baroclinic systems, since they are low level processes, and their relationship with the wave trains shows that they occur when the atmosphere is baroclinically unstable. Only about 20% of them are associated with TTTs, whereas almost all the TTTs are followed by ridging highs, a finding which has been enabled by the objective identification of both processes. This sequence of events plays an important role in the moisture transport during the evolution of TTTs. This transport starts off as southeastward, thus bringing moisture towards South Africa from the tropical Atlantic Ocean (Viguad et al. 2007) around the Angola low (Rouault et al. 2003; Reason and Jagadheesha 2005; Reason et al. 2006; Howard and Washington 2018). At later stages of the TTTs, the ridging highs bring moisture from the SWIO. This feature is not observed in the Macron et al. (2014) analysis but it is evident in the composites of low level flow in Ratna et al. (2013). This means that when ridging highs are linked to TTTs, they contribute to the mechanism that links tropical and temperate processes that are well known to be characteristic of TTTs. This issue had not been made explicit in previous studies.

Before the inception of the ridging process, there is a pre-existing north-eastern high pressure system that is located over the north eastern parts of South Africa and southern Mozambique. This high pressure system is a synoptic-scale climatological feature. Its climatological presence gives rise to moisture fluxes in the southern Mozambique region, as seen in previous studies (e.g., Viguad et al. 2007). However, the composite analyses employed in this

study reveals that the climatology of this high pressure system, as well as the flow and the moisture fluxes associated with it are affected by ridging highs. When the ridging process commences, the high pressure weakens significantly and almost vanishes, and it is re-established again as the South Atlantic Ocean anticyclones extend eastward, wrap around the country and entering the country over the eastern parts. This intrusion into land also induces a positive geopotential tendency field, which in turn informs the direction of the ageostrophic flow, with the Eulerian acceleration of the geostrophic flow informing its magnitude. The ageostrophic flow is largely onshore right through the evolution of ridging, south of the 30°S latitude line, whilst the geostrophic flow is largely parallel to the south eastern coast during the early stages and becomes strongly onshore over southern Mozambique, at the later stages of the evolution of ridging highs. The ageostrophic flow also follows the coast on land (i.e. northeastward) and therefore enters the north-eastern high pressure system from the south. On the northern side of the high pressure system, the direction of the ageostrophic flow is northwestward to southeastward, thus rendering it almost perpendicular to the geostrophic flow that approaches from the east. These flow vectors directly influence the moisture fluxes, with the ageostrophic fluxes approaching the north-eastern parts of South Africa from the south, whilst the geostrophic fluxes approach from the east, where they have entered the country from the Mozambique Channel.

A summary of the moisture fluxes identified in this study is presented in the schematic diagram shown in Figure 8. By dividing the flow and moisture fluxes into their ageostrophic (red arrows in Figure 8) and geostrophic (blue arrows in Figure 8) components, the composite analysis employed in this study has been able to show that moisture that is brought by ridging highs into the country originates from different parts of the Indian Ocean at different times steps of its evolution. Moisture is added by the ridging process from the Mozambique Channel and this moisture accumulates over the north eastern parts of South Africa, Swaziland and southern Mozambique and leads to large rainfall anomalies in Mozambique. Previous studies have not pointed out the dynamical nature of the moisture fluxes that dominate in those regions. We have shown here that it is geostrophic flow processes that are dominant in that part of the sub-continent. The other contribution of this study was to show that it is not sufficient to consider the moisture fluxes by the total flow, because the accumulation of moisture in the over the eastern half of South Africa, in particular in the province of KwaZulu Natal, is otherwise difficult to explain. It is when ageostrophic moisture fluxes (see long red arrow in Figure 8) are considered, as proposed in this study, in the analysis that it becomes apparent that this moisture originates from the SWIO that is adjacent to the country, along the south eastern and eastern coasts of South Africa. It has been demonstrated that the ageostrophic moisture fluxes play a more critical role in moisture transport into this part of South Africa, which has important implications for weather forecasting in the region. Through a combination of ageostrophic and geostrophic flows, moisture accumulates over the north eastern parts of South Africa as well as the southern parts of Mozambique.

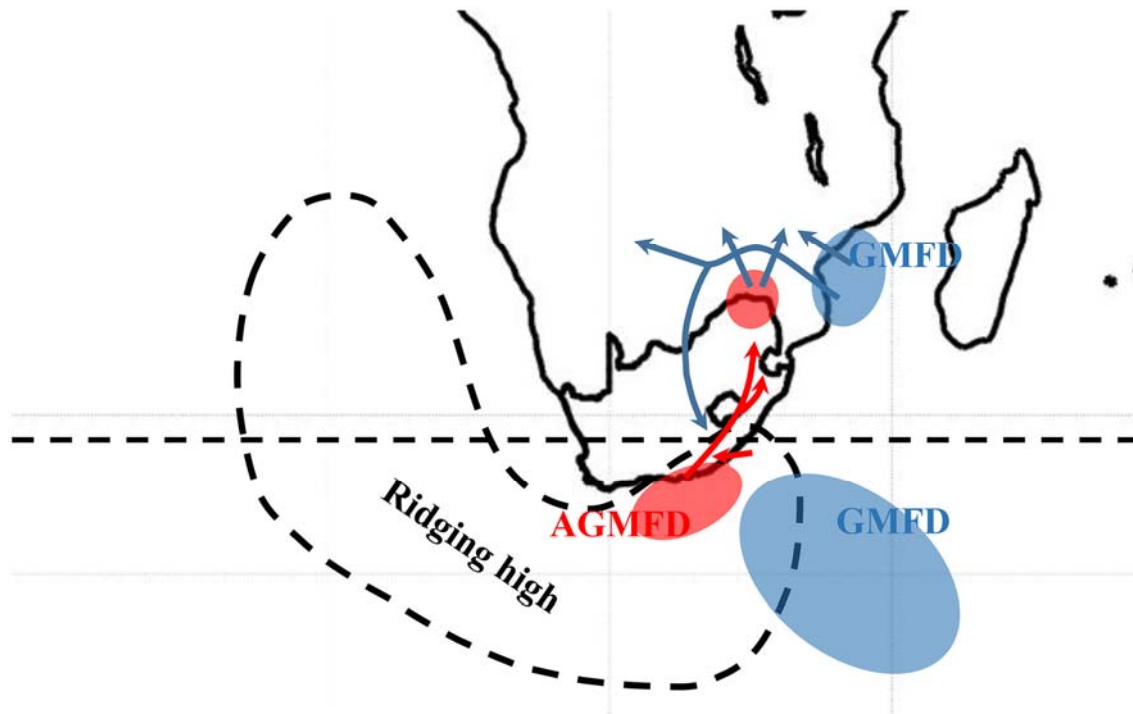


FIGURE 8. Schematic summary of ageostrophic (red arrows) and geostrophic (blue arrows) moisture fluxes. The red and blue shaded areas represent the ageostrophic (AGMFD) and geostrophic moisture flux divergence (GMFD), respectively. The dashed contour represent a mean sea level pressure contour depicting a ridging South Atlantic Ocean anticyclone and the red dashed line represent the 30S latitude line

There is some indication of areas that appear to be preferred sources of moisture in the SWIO, which are highlighted by the separating the divergence of the fluxes into ageostrophic and geostrophic components. The former is concentrated along the coastal areas (red shaded area near the coast in Figure 8), whilst the latter is located further afield into the ocean (blue shaded region in Figure 8), and is always ahead as ridging evolves. Another geostrophic moisture source is located in the Mozambique Chanel. However, moisture divergence is not sufficient for completely diagnosing these sources. Such an analysis can be obtained through the use of Lagrangian models (e.g., Stohl and James, 2004) and the identification of moisture sources and sinks, as well as moisture trajectories that eventually end up in southern Africa from the surrounding oceans. A recent paper in *Climate Dynamics* (Rapolaki et al 2020) has applied Lagrangian trajectory analyses to the Limpopo River Basin region of southern Africa.

The objective identification of ridging highs proposed in this study enables us to quantify the contribution of these rainfall systems to summer rainfall. We find that they are associated with 60% of rainfall days during the summer rainfall season per year, whilst TTTs are associated with 21% of summer rainfall days. The rainfall that is directly associated with ridging highs is mainly confined to the coast, perhaps due to orographic features at and near the coast. At the early stages of the ridging process it is found along the south and south eastern coasts, where it is largely caused by moisture in flux that is facilitated by the ageostrophic flow. After having migrated northward tracing the coast towards Mozambique to reach a maximum there, it is influenced by geostrophic processes.

ACKNOWLEDGEMENTS

This study was partially supported by the Water Research Commission (Project number K5/2829), the authors would also like to thank Prof. Darryn Waugh for commenting on the manuscript and the anonymous reviewers.

Endnote

¹ <https://www.esrl.noaa.gov/psd/>

REFERENCES

- Abram, N.J., Mulvaney, R., Vimeux, F., Phipps, S.J., Turner, J. and England, M.H. (2014) Evolution of the 14 southern annular mode during the past millennium. *Nature Climate Change*, 4, 564– 569.15. <https://doi.org/10.1038/nclimate2235>.
- Ambrizzi, T., Hoskins, B.J. and Hsu, H.-H. (1995) Rossby wave propagation and teleconnection patterns in the austral winter. *Journal of the Atmospheric Sciences*, 52, 3 661– 3 3672.
- Barimalala, R., Desboilles, F., Blamey, R.C. and Reason, C.J.C. (2018) Madagascar influence on the South Indian Ocean convergence zone, the Mozambique Channel trough and southern African rainfall. *Geophysical Research Letters*, 45, 11380 – 11389.
- Barimalala, R., Blamey, R.C., Desboilles, F. and Reason, C.J.C. (2020) Variability in the Mozambique Channel trough and impacts on southeast African rainfall. *Journal of Climate*, 33, 749– 765.
- Behera, S.K., Krishnan, R. and Yamagata, T. (1999) Unusual Ocean-atmosphere conditions in the tropical Indian Ocean during 1994. *Geophysical Research Letters*, 26, 3001– 3004.
- Blackburn, W. (1985) Interpretation of ageostrophic winds and implications for jet stream maintenance. *Journal of the Atmospheric Sciences*, 42(23), 2604– 2620.
- Blamey, R.C. and Reason, C.J.C. (2009) Numerical simulation of a mesoscale convective system over the east coast of South Africa. *Tellus*, 61, 17– 34.
- Blamey, R.C. and Reason, C.J.C. (2012) Mesoscale convective complexes over southern Africa. *Journal of Climate*, 25, 753– 766.
- Brown, T.J. and Hall, B.L. (1999) The use of t values in climatological composite analyses. *Journal of Climate*, 12, 2941– 2944.
- Chen, T-G. (1985) Global water vapour flux and maintenance during FGGE. *Monthly Weather Review*, 113, 1801– 1819.
- Chikoore, H., Vermeulen, J.H. and Jury, M.R. (2015) Tropical cyclone in Mozambique Channel: January–march 2012. *Natural Hazards*, 77(3), 2081– 2095. <https://doi.org/10.1007/s11069-015-1691-0>.

- Cook, K.H. (1999) Generation of the African easterly jet and its role in determining west. *Africa. \it Journal of Climate*, 12, 1165– 1183.
- Cook, C., Reason, C.J.C. and Hewitson, B.C. (2004) Wet and dry spells within particularly wet and particularly dry summers in the south African summer rainfall region. *Climate Research*, 26, 17– 31.
- Crétat, J., Pohl, B., Dieppois, B., Berthou, S. and Perguad, J. (2019) The Angola Low: relationship with southern African rainfall and ENSO, 52, 1783–1803.
- Crimp, S.J. and Mason, S.J. (1999) The extreme precipitation event of 11 to February 16, 1996 over South Africa. *Meteorology and Atmospheric Physics*, 70, 29– 42.
- D’Abreton, P.C. and Lindesay, J.A. (1993) Water vapour transport over southern Africa during wet and dry early and late summer months. *International Journal of Climatology*, 13, 151– 170.
- D’Abreton, P.C. and Tyson, P.D. (1995) Divergent and non-divergent water vapour transport over southern Africa during wet and dry conditions. *Meteorology and Atmospheric Physics*, 55, 47– 59.
- de Coning, E. (2013) Optimizing satellite-based precipitation estimation for Nowcasting of rainfall and flash flood events over the south African domain. *Remote Sensing*, 5, 5702– 5724.
- Dee, D.P., Uppala, S.M., Simmons, A.J., Berrisford, P., Poli, P., Kobayashi, S., Andrae, U., Balmaseda, M.A., Balsamo, G., Bauer, P., Bechtold, P., Beljaars, A.C., van de Berg, L., Bidlot, J., Bormann, N., Delsol, C., Dragani, R., Fuentes, M., Geer, A.J., Haimberger, L., Healy, S.B., Hersbach, H., Hólm, E.V., Isaksen, L., Kállberg, P., Köhler, M., Matricardi, M., McNally, A.P., Monge-Sanz, B.M., Morcrette, J., Park, B., Peubey, C., de Rosnay, P., Tavolato, C., Thépaut, J. and Vitart, F. (2011) The ERA-interim reanalysis: configuration and performance of the data assimilation system. *Quarterly Journal of the Royal Meteorological Society*, 137, 553– 597.
- Dessler, A.E. and Davis, S.M. (2010) Trends in tropospheric humidity from reanalysis systems. *Journal of Geophysical Research*, 115, D19127.
<https://doi.org/10.10129/2010JD014192>.
- Doswell, C.A., III, Brooks, H.E. and Maddox, R.A. (1996) Flash flood forecasting: an ingredients-based methodology. *Weather and Forecasting*, 11, 560– 580.
- Dyson, L. (2015) A heavy rainfall sounding climatology over Gauteng South Africa, using self-organising maps. *Climate Dynamics*, 45, 3051– 3065.
- Engelbrecht, C.J., Landman, W.A., Engelbrecht, F.A. and Malherbe, J. (2015) A synoptic decomposition of rainfall over the cape south coast of South Africa. *Climate Dynamics*, 44, 2589– 2607.

Favre, A., Hewitson, B., Lennard, C., Cerezo-Mota, R. and Tadorss, M. (2013) Cut-off Lows in the South Africa region and their contribution to precipitation. *Climate Dynamics*, 41, 2331– 2351.

Fauchereau, N., Pohl, B., Reason, C.J.C., Rouault, M. and Richard, Y. (2009) Recurrent daily OLR patterns in the southern Africa/Southwest Indian Ocean region, implications for south African rainfall and teleconnections. *Climate Dynamics*, 32, 575– 591.

Funk C., Hoell A., Shukla S., Husak G., and Michaelsen J. (2016) The east African monsoon system: Seasonal Climatologies and recent variations. In: de L. Carvalho, C. Jones (eds) *The Monsoons and Climate Change*. Springer Climate. Springer, Cham.

Hart, N.C.G., Reason, C.J.C. and Faucherau, N. (2010) Tropical-extratropical interactions over southern Africa: three cases of heavy summer season rainfall. *Monthly Weather Review*, 138, 2608– 2623.

Holton, J.R. and Hakim, G.J. (2013) *An Introduction to Dynamic Meteorology*, Vol. 553, 4th edition. Oxford: Elsevier Academic Press.

Holton, J.R. and Hakim, G.J. (2014) *An Introduction to Dynamic Meteorology*, 5th edition. Elsevier Academic Press, 553 pp.

Howard, E. and Washington, R. (2018) Characterizing the synoptic expression of the Angola Low, 31, 7147–7165.

Kobayashi, S., Ota, Y., Harada, Y., Ebata, A., Moriya, M., Onoda, H., Onogi, K., Kamahori, H., Kobayashi, C., Endo, H., Miyaoka, K. and Takahashi, K. (2015) The JRA-55 reanalysis: general specifications and basic characteristics. *Journal Meteorological Society of Japan*, 93, 5– 48. <https://doi.org/10.2151/jmsj.2015-001>.

Kwon, H.J. and Lim, G.-H. (1999) Reexamination of the structure of the ageostrophic wind in baroclinic waves. *Journal of the Atmospheric Sciences*, 56, 2512– 2521.

Lim, G.-H., Holton, J.R. and Wallace, J.M. (1991) The structure of the ageostrophic wind field in baroclinic waves. *Journal of the Atmospheric Science*, 48(15), 1733– 1745.

Macron, C., Pohl, B. and Richard, Y. (2014) How do tropical temperate troughs form and develop over southern Africa. *Journal of Climate*, 27, 1633– 5199.

Mahlalela, P.T., Blamey, R.C. and Reason, C.J.C. (2019) Mechanisms behind early winter rainfall variability in the southernwestern cape, South Africa. *Climate Dynamics*, 53, 21– 39.

Malherbe, J., Engelbrecht, F.A., Landman, W.A. and Engelbrecht, C.J. (2012) Tropical systems from the Southwest Indian Ocean making landfall over the Limpopo River basin, southern Africa: a historical perspective. *International Journal of Climatology*, 32, 1018– 1032. <https://doi.org/10.1002/joc.2320>.

Malherbe, J., Landman, W.A. and Engelbrecht, F.A. (2014) The bi-decadal rainfall cycle southern annular mode and tropical cyclones over the Limpopo River basin, southern Africa. *Climate Dynamics*, 42, 3121– 3138. <https://doi.org/10.1007/s00382-013-2027-y>.

- Ndarana, T., Bopape, M., Waugh, D. and Dyson, L. (2018) The influence of the lower stratosphere on ridging Atlantic Ocean anticyclones over South Africa. *Journal of Climate*, 31, 6175– 6187.
- O'Brien, L. and Reeder, M.J. (2017) Southern Hemisphere summertime Rossby waves and weather in the Australian region. *Quarterly Journal of the Royal Meteorological Society*, 143, 2374– 2388.
- O'Kane, T.J., Risbey, J.S., Monselesan, D.P., Horenko, T. and Franzke, C.L.E. (2016) On the dynamics of persistent states and their secular trends in the wave guides of the southern hemisphere troposphere. *Climate Dynamics*, 46, 3567– 3597.
- Piva, E.D., Gan, M.A. and Rao, V.B. (2010) Energetics of winter troughs entering South America. *Monthly Weather Review*, 138, 1084– 1103.
- Rapolaki, R.S., Blamey, R.C., Hermes, J.C. and Reason, C.J.C. (2019) A classification of synoptic weather patterns linked to extreme rainfall over the Limpopo River basin in southern Africa. *Climate Dynamics*, 53, 2265– 2279.
- Rapolaki, R.S., Blamey, R.C., Hermes, J.C. and Reason, C.J.C. (2020) Moisture sources associated with heavy rainfall over the Limpopo River Basin, southern Africa. *Climate Dynamics*. <https://doi.org/10.1007/s00382-020-05336-w>.
- Ratna, S.B., Behera, S., Ratnam, J.V., Takahashi, K. and Yamagata, T. (2013) An index for tropical temperate troughs over southern Africa. *Climate Dynamics*, 41, 421– 441.
- Ratna, S.B., Ratnam J.V., Behera S.K., deW. Rautenbacht C.J., Ndarana T., Takahashi K. and Yamagata, T. (2014) Performance assessment of three convective parameterization schemes in WRF for downscaling summer rainfall over South Africa. *Climate Dynamics*, 42, 2931– 2953.
- Reason, C.J.C. and Jagadheesha, D. (2005) A model investigation of recent ENSO impacts over southern Africa. *Meteorology and Atmospheric Physics*, 89, 81– 205.
- Reason, C.J.C., Landman, W. and Tennant, W. (2006) Seasonal to decadal prediction of southern African climate and its links with variability of the Atlantic Ocean. *Bulletin of the American Meteorological Society*, 87, 941– 956.
- Roffe, S.J., Fitchett, J.M. and Curtis, C.J. (2019) Classify and mapping rainfall seasonality in South Africa: a review. *South African Geographical Journal*, 101(2), 158– 174.
- Rouault, M., Florenchie, P., Fauchereau, N. and Reason, C.J.C. (2003) South east tropical Atlantic warm events and southern African rainfall. *Geophysical Research Letters*, 30(5). <https://doi.org/10.1029/2002GL014840>.
- Singleton, A.T. and Reason, C.J.C. (2007) A numerical study of an intense cut-off low pressure system over South Africa. *Monthly Weather Review*, 135, 1128– 1150.

- Stohl, A. and James, P. (2004) A Lagrangian analysis of the atmospheric branch of the global water cycle, part 1: method description, validation and demonstration for the august 2002 flooding in Central Europe. *Journal of Hydrometeorology*, 5, 656– 678.
- Suzuki, T. (2011) Seasonal variation of the ITCZ and its characteristics over Central Africa. *Theoretical and Applied Climatology*, 103, 39– 60.
- Todd, M.C., Washington, R. and Palmer, P.I. (2004) Water vapour transport associated with tropical-temperate trough systems over southern Africa and the South West Indian Ocean. *International Journal Climatology*, 24, 555– 568.
- Triegaardt, D.O., Terblanche, D.E., van Heerden, J. and Laing, M.V. (1988) The Natal flood of September 1987. South African Weather Bureau Tech. Paper 19, 62 pp. [Available from the South African Weather Service, Private Bag x097, Pretoria, 0001, South Africa.]
- Vigaud, N., Pohl, B. and Crétat, J. (2012) Tropical-temperate interactions over southern Africa simulated by a regional climate model. *Climate Dynamics*, 39, 2895– 2916.
- Vigaud, N., Richard, Y., Rouault, M. and Fauchereau, N. (2007) Water vapour transport from the tropical Atlantic and summer rainfall in tropical southern Africa. *Climate Dynamics*, 28, 113– 123.
- Xue, M., Luo, X., Zhu, K., Sun, Z. and Fei, J. (2018) The controlling role of boundary layer inertial oscillations in Meiyu front precipitation and its diurnal cyclones over China. *Journal Geophysical Research Atmospheres*, 123, 5090– 5115.
- Weldon, D. and Reason, C.J.C. (2014) Variability of rainfall characteristics over the south coast region of South Africa. *Theoretical and Applied Climatology*, 115, 177– 185.
- Zheng, F., Li, J., Clark, R.T. and Nnamchi, H.C. (2013) Simulation and projection of the southern hemisphere annular mode in CMIP5 models. *Journal of Climate*, 26, 9860– 9879. <https://doi.org/10.1175/JCLI-D-13-00204.1>.